Ann. Geophys., 29, 1037–1048, 2011
www.ann-geophys.net/29/1037/2011/
doi:10.5194/angeo-29-1037-2011

Annales Geophysicae

Average properties and small-scale variations of the mesospheric Na and Fe layers as observed simultaneously by two closely colocated lidars at 30° N

L. Chen and F. Yi

School of Electronic Information, Wuhan University, China

Key Laboratory of Geospace Environment and Geodesy, Ministry of Education, Wuhan, China

State Observatory for Atmospheric Remote Sensing, Wuhan, China

Received: 20 March 2011 – Revised: 2 June 2011 – Accepted: 7 June 2011 – Published: 16 June 2011

Abstract. We report the average properties and small-scale variation features of the mesospheric Na and Fe layers at 30° N from extensive simultaneous and common-volume Na and Fe lidar measurements at Wuhan, China. The annual mean Na and Fe density profiles are derived in terms of an averaging method taken from an early literature. The mean Na and Fe profiles preserve the sharp gradients present in most individual density profiles near the layer bottom. Near the bottommost of the layers the mean Na and Fe scale heights are respectively −0.42 and −0.30 km. The mean layer parameters coincide well with the previous report. The Na and Fe densities in the lowest several kilometers of the layers consistently exhibit nearly the same time variations. A clear-cut distinction between the Na and Fe time variations always appears in an altitude range near 90 km. A relatively weak positive correlation between them persistently occurs also in an altitude range near 100 km. The mean increase and decrease rates for both Na and Fe are altitude dependent and have a single-peak structure. The time constant of the layer variation is ∼0.07–2.0 h for Na and ∼0.02–1.7 h for Fe, suggesting that the variability is dominated by small-scale processes. However, there is also a slow net increase in each of the annual mean column abundances (Na and Fe) during night.

Keywords. Atmospheric composition and structure (Middle atmosphere – composition and chemistry)

Correspondence to: F. Yi
(yf@whu.edu.cn)

1 Introduction

Free metal atom layers (Na, Fe, K, Ca, and Li), residing in the mesosphere/lower thermosphere (MLT) region from 80 to 110 km, have been detected with ground-based lidar for over 40 years (Bowman et al., 1969). Meteoric ablation is believed to provide the substance source for the metal layers. Based on independent extensive lidar measurements, the average properties and seasonal variations of these layers have been respectively obtained at many locations (Megie and Blamont, 1977; Clemesha et al., 1979; Simonich et al., 1979; States and Gardner, 1999; Plane et al., 1999b; Eska et al., 1999; Gerding et al., 2000; She et al., 2000; Gardner et al., 2005, 2011; Yi et al., 2009). Several one-dimensional gas-phase chemical models corresponding to different metal species such as Na, Fe, K, and Ca have been respectively developed to explain these observational results (Helmer et al., 1998; Plane et al., 1999b; Eska et al., 1999; Gerding et al., 2000; Plane, 2004; Gardner et al., 2005). All the models start with the conventional continuity equation, which assume (require) that the meteoric influx for each gas-phase metal species (e.g., Na or Fe) is balanced by its downward transport via eddy diffusion and/or net vertical wind under time-averaged condition. The Na and Fe models among others can reproduce some primary features of the normal Na and Fe layers observed at midlatitudes (Helmer et al., 1998; Plane et al., 1999b), such as the layer shapes and the seasonal variations in the layer parameters. However, some unsolved pivotal problems in understanding the entire chain of processes and reactions resulting to the metal atom layers are still puzzling us. For instance, how large is the actual magnitude of the gas-phase metal (e.g., Na or Fe) input flux from meteoric ablation (as yet there is no direct or indirect

Published by Copernicus Publications on behalf of the European Geosciences Union.

measurement for the total vertical flux of any mesospheric metal species produced by meteoric ablation)? What subset of the mass/velocity/mass density distribution of the entering micrometeoroids contributes actually to the observed metal layers? The residence time for a typical metal atom in the layer is really as long as several days? Clarifying these problems obviously needs further observational and modeling efforts.

Since the mesospheric metal layers are influenced by input of gas-phase metal materials from meteoric ablation, chemical reactions, and dynamics, exploring the relationship between various layers may provide some new insights into the complicated layer processes. According to the existing lidar observations, Fe is the most abundant of the mesospheric metallic atoms (Bills and Gardner, 1990; Alpers et al., 1990). This is consistent with the fact that Fe is the main component of the meteoric source, whereas the alkali metals are the minor ones (Heide and Wlotzka, 1995). Among the alkali metals, only the Na layer has a typical abundance value approaching that of the Fe layer (Kane and Gardner, 1993; Gardner et al., 2005; Yi et al., 2009). Hence a detailed quantitative comparison between the Na and Fe layers at a given site is feasible. Kane and Gardner (1993) compared the Na and Fe layer data obtained simultaneously by two lidars at a midlatitude site (40° N). They noticed that even though the individual density profiles appeared quite different, the temporal variations of Na and Fe layer parameters (abundances, centroid heights, and RMS widths) were highly correlated in most cases. The simultaneous and common-volume Na and Fe lidar observations at 30° N revealed that Na and Fe lower boundaries always follow almost the same track and show consistently a delicate stratification with the Fe lower boundary being in general slightly higher than or coincident with that of the Na layer (Yi et al., 2007, 2008). In addition, the Na layer always shows a few kilometers more extension on its top side than the Fe layer. These features can be seen also from a comparison of simultaneously observed Na and Fe layers at high, mid, and low latitudes respectively (Kane and Gardner, 1993; Lynch et al., 2005; Shibata et al., 2006), which may be universal. They provide a connection between the two different metallic species in the mesopause region. In this paper, we first derive the mean profiles of the Na and Fe layers based on the more extensive data from the simultaneous and common-volume Na and Fe lidar measurements at our 30° N lidar site. The mean profiles will quantitatively show the relationship of the two background metal layers. In contrast to our previous work that only focuses on the relationship between the Na and Fe layer boundaries (defined by a given small density criterion) (Yi et al., 2008), here we will examine the relation between the Na and Fe density variations at all fixed altitudes over the main metal layer. An intriguing ubiquitous connection between the Na and Fe density variations at fixed altitudes on the layer bottom side is revealed for the first time. It provides a new clue for understanding the basic processes inherent to the meteoric metal layers. Finally, the mean increase and decrease rate profiles for the Na and Fe layers are derived to give an insight into the Na and Fe variability.

2 Observational results

The Na and Fe density data reported here come from the simultaneous and nearly common-volume Na and Fe lidar measurements at Wuhan from March 2004 to December 2008. For the purposes of this study, we start from the Na and Fe photon count profiles with an altitude resolution of 96 m and a time resolution of 5 min (the 5-min photon count profiles are obtained simply by cumulating the corresponding 4-s profiles when the raw lidar data were collected with a time resolution of 4 s (Liu and Yi, 2009)). The Na and Fe density profiles are derived from the corresponding lidar photon count profiles by using a standard method (Gardner, 1989). The normalization altitude is taken to be 30 km. For guaranteeing a good data quality, all the 5-min density data used here are required to have the detection thresholds less than 200 cm^{-3} in the entire altitude range of the metal layers (75–110 km). The sporadic Na and Fe layers are often observed at our lidar site near 30° N (Yi et al., 2002, 2007; Ma and Yi, 2010). They are characterized by a large density enhancement in a narrow altitude range and have no clear-cut relation with the main metal layers. The present study is only concerned with the average properties and small-scale variations of the main metal layers, consequently those profiles containing such sporadic layers have been excluded from the Na and Fe data. The remaining data represent ∼268 h simultaneous Na and Fe measurements on 47 different nights. The 47 nights of the simultaneous Na and Fe data have a complete month coverage (with at least one night of the data each month). The data duration per night is larger than 3 h. Thus, the present data set displays more extensive observations than that in our earlier report (Yi et al., 2008).

2.1 Mean Na and Fe density profiles

Figure 1 gives two typical examples of the individual 5-min Na and Fe density profiles on 29 July 2004 and 9 December 2004. Despite the fact that the two pairs of the Na and Fe density profiles are respectively from summer and winter, some shared features can be discerned: both the Na and Fe layers have much steeper density gradients on the bottom side than on the top side, and the borders of the Fe layer are obviously steeper than those of the Na layer. In addition, the upper boundary of the Na layer is a few kilometers higher than that of the Fe layer, while the lower boundary of the Na layer is several hundred meters lower than that of the Fe layer. Like our previous report (Yi et al., 2008), these features are actually common for most individual Na and Fe density profiles obtained from our simultaneous and common-volume Na and Fe lidar measurements.

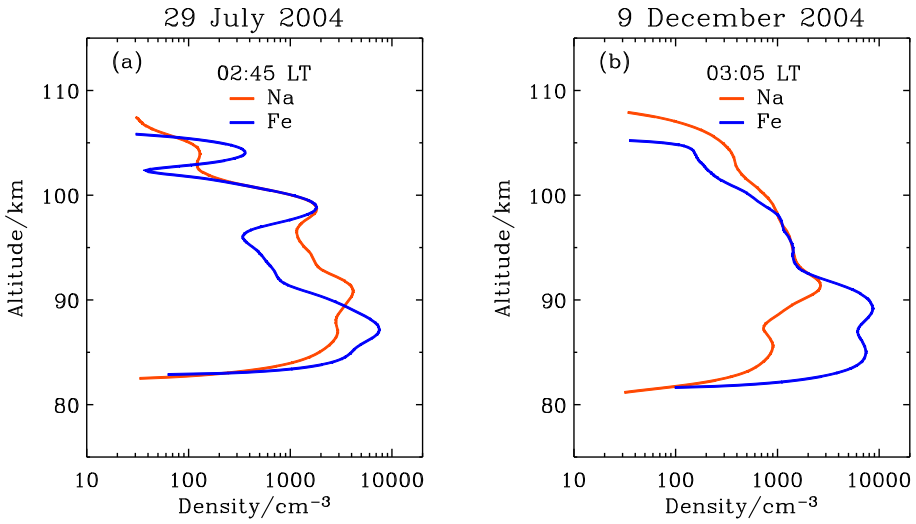

Fig. 1. Simultaneous 5-min Na and Fe density profiles measured at **(a)** 02:45 LT on 29 July 2004 and **(b)** 03:05 LT on 9 December 2004. The two examples represent some ubiquitous features of simultaneously observed Na and Fe layers: the upper boundary of the Na layer is a few kilometers higher than that of the Fe layer, while the lower boundary of the Na layer is several hundred meters lower than that of Fe layer. Both the Na and Fe layers have much steeper density gradients on the bottom side than on the top side, and the borders of the Fe layer are obviously steeper than those of the Na layer. Note the density criterion is taken to be 30 cm^{-3} uniformly for both Na and Fe according to their thresholds.

Now let us derive the annual mean Na and Fe density profiles from the ∼268 h concurrent Na and Fe density data. We want to calculate a composite profile that preserves the sharp gradients present in most individual density profiles. Noting a fact that the altitudes of the Na and Fe layer bottoms often show considerable displacements on small time scale (Tilgner and von Zahn, 1988; Yi et al., 2008), an averaging approach developed by Tilgner and von Zahn (1988) is used here. In this approach, the average calculation is performed by taking a median value instead of the conventional arithmetic mean because it ignores possible extreme density value (Tilgner and von Zahn, 1988). The starting point (altitude) and ending point (altitude) of a given (Na or Fe) density profile are confined by the magnitudes of the detection thresholds at such points (altitudes). In order to reduce the detection thresholds, we adopt in this average calculation the photo count profiles after integration over 15 min, that are obtained simply by adding three adjacent raw 5-min profiles. Thus, the total of ∼268 h of simultaneous Na and Fe lidar data are composed of 1073 pairs of the 15-min Na and Fe density profiles. In terms of our calculation, the maximum detection threshold at 110-km altitude is ∼67 cm^{-3} for all the 15-min Na and Fe density profiles, while the corresponding quantity at 85-km altitude is 40 cm^{-3}. Hence, the density criteria for the high and low boundaries of the 15-min Na and Fe density profiles are respectively set to 70 and 40 cm^{-3}. The nightly mean Na and Fe density profiles are derived following the averaging approach of Tilgner and von Zahn (1988). The annual mean Na and Fe density profiles are then deduced from the 47 pairs of the nightly mean Na and Fe profiles by the same way as that used in deriving the nightly mean profile. Figure 2 gives the annual mean Na and Fe profiles derived by the averaging approach of Tilgner and von Zahn (1988). Note that the profiles have been smoothed with a running mean over ∼1.2 km (12 altitude bins) in altitude. As seen in Fig. 2, the mean Na and Fe profiles preserve those essential features seen in most individual pairs of the 5-min Na and Fe profiles (e.g., both the Na and Fe layers have much steeper density gradients on the bottom side than on the top side, and the borders of the Fe layer are obviously steeper than those of the Na layer). Hence, the profiles shown in Fig. 2 represent the actual annual mean Na and Fe density profiles from the simultaneous and common-volume lidar measurements at 30° N. According to Fig. 2, the Na column abundance, centroid height and RMS width are respectively 2.8×10^9 cm^{-2}, 91.5 km, and 4.1 km, while the corresponding values for Fe are respectively 7.4×10^9 cm^{-2}, 88.8 km, and 3.6 km (see Table 1). The values of the column abundance and centroid height approach those derived in terms of the conventional arithmetic mean from the more extensive Na and Fe lidar measurements (including separate Na and Fe data) at Wuhan (Yi et al., 2009), while the values of the RMS width are slightly smaller than those given by Yi et al. (2009). This is caused by the detection threshold criteria imposed on the layer boundaries.

The Na and Fe density scale heights are calculated based on the data in Fig. 2 and shown in Fig. 3. For comparison, the profiles of the background atmospheric scale height and the natural scale heights (diffusive equilibrium scale heights) for Na and Fe atoms are also plotted in Fig. 3. As seen in Fig. 3,

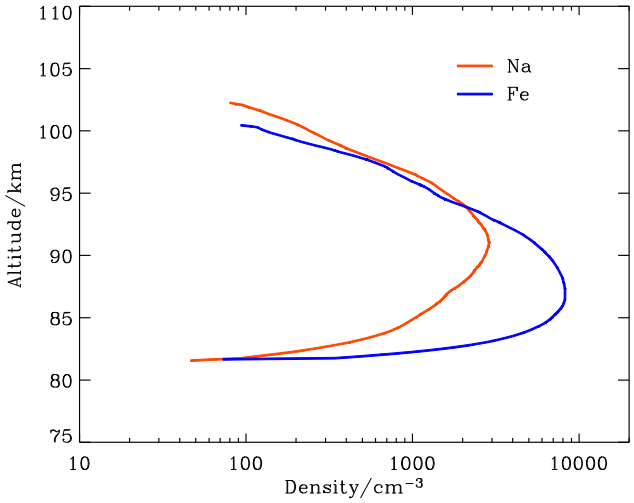

Fig. 2. Annual mean Na and Fe profiles derived based on a total of ∼268 h of simultaneous and nearly common-volume Na and Fe lidar measurements from March 2004 to December 2008 at 30° N (the averaging method is depicted in text). The profiles have been smoothed with a running mean over 1.2 km in altitude. Note that the mean Na or Fe density profile can preserve the sharp gradients present in most individual density profiles near the layer bottom.

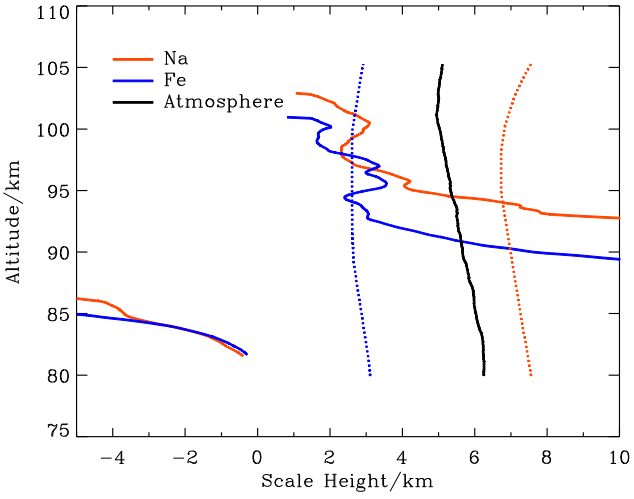

Fig. 3. Profiles of Na and Fe density scale heights (orange and blue solid lines) as calculated from Fig. 2. The profiles have been smoothed with a running mean over 1.2 km in altitude. For comparison, profiles of the atmospheric scale height (black solid line) and natural scale heights for Na (orange dotted line) and Fe (blue dotted line) atoms are also given. The Na scale height has a minimum (absolute value) of −0.42 km at the lowest point of the layer, while for Fe this value is −0.30 km. On the layer upper side, the Na scale height has a value of ∼1.06 km at the highest point of the layer, while for Fe this value is ∼0.82 km.

Table 1. Parameters of the mean Na and Fe density profiles.

	Mean Na layer	Mean Fe layer
Column density (10^9 cm^{-2})	2.8	7.4
Centroid height (km)	91.5	88.8
RMS width (km)	4.1	3.6
Peak density (cm^{-3})	2842	8179
Peak height (km)	91.6	87.1
Halfwidth (FWHM) of the layer (km)	9.8	8.9

both the bottom sides of the mean Na and Fe layers exhibit very small scale heights (absolute values) with the magnitude of the Fe scale height mostly being slightly smaller than that of Na. In particular, the Na scale height has a minimum (absolute value) of −0.42 km at the lowest point of the layer, while for Fe this value is −0.30 km. The magnitude of the Na scale height approaches that value (−0.4 km) derived by Tilgner and von Zahn (1988) based on the wintertime Na lidar observations at 69° N. Note that both the scale heights on the bottom sides of the Na and Fe layers are obviously smaller in magnitude than those derived from the conventional arithmetic average (<2 km for Na and <1 km for Fe) (Plane, 2003). On the layer underside, the magnitudes of the Na and Fe scale heights both increase rapidly with increasing altitude. On the top side, the Na and Fe layers both have somewhat larger scale heights than their counterparts on the underside, which is consistent with the feature seen from most individual Na and Fe density profiles. The Na scale height decreases from 4.46 km at an altitude of 95 km to 1.06 km around an altitude of 103 km, while for Fe it decreases from 2.74 km at an altitude of 95 km to 0.82 km near an altitude of 101 km. On the basis of the extensive data from the simultaneous and common-volume Na and Fe lidar measurements, it can be firmly said that on both the bottom and top sides of the layer, the observed density scale height (in magnitude) for Fe is generally smaller than for Na. This result is coincident with that derived from the less extensive Na and Fe data (Yi et al., 2008). It is noted from Fig. 3 that on the top sides of the Na and Fe layers, the observed scale heights are obviously smaller than their (Na and Fe) natural scale heights as well as the background atmospheric scale height. On the layer top side near 102-km altitude, the diffusion for each metal constituent is believed to be influenced by both molecular and eddy effects. Molecular diffusion tends to drive the density falloff of any given constituent to its natural scale height, while eddy diffusion tends to drive the density falloff to the background atmospheric scale height (Heinselman, 1999). Therefore, we believe that the altitude variation in Na and Fe densities on the layer top side must represent some features of source and/or sink for Na and Fe atoms as conjectured earlier by Tilgner and von Zahn (1988). On the bottom sides of the Na and Fe layers, the consistently negative and small values of the measured Na and Fe scale heights reflect the significant gradients in the source and/or sink for Na and Fe atoms on the layer bottom.

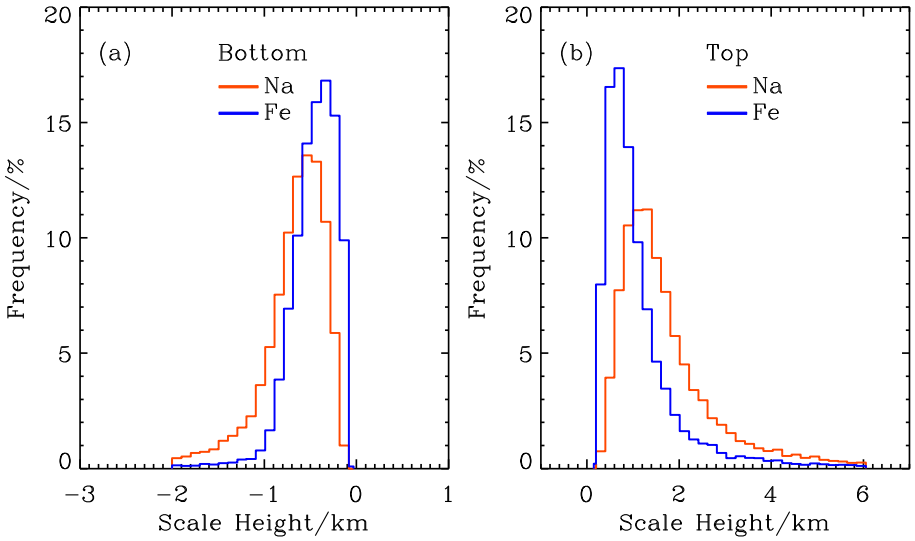

Fig. 4. Distribution of Na and Fe number density scale heights for the layer bottom (ten consecutive points lowest in altitude) and top (ten consecutive points highest in altitude) from the 1073 pairs of the 15-min Na and Fe density profiles measured simultaneously on 47 different nights at 30° N.

Figure 4 presents the distributions of the Na and Fe density scale heights on the layer bottom sides (ten consecutive points lowest in altitude) and on the layer top sides (ten consecutive points highest in altitude), which come from the 1073 pairs of the 15-min Na and Fe density profiles from the simultaneous and common-volume Na and Fe lidar measurements at Wuhan. Figure 4a exhibits that 94 % and 98 % of all the Na and Fe scale height values (10 730 pairs) on the layer bottom side are distributed in a range between −2 and −0.05 km. As shown in Fig. 4b, 93 % of both the Na and Fe scale height values on the layer top side lie in a range of 0.15–6 km. Figure 4a and b statistically illustrates that both the Na and Fe layers generally have evidently smaller density scale heights on the bottom side than on the top side. In addition, the distributions of the Na scale height values on both the layer bottom and top sides are as a whole shifted towards the large scale height direction (in magnitude) compared with those of the Fe values. The distribution peaks on the layer bottom sides are respectively at −0.5 to −0.6 km for Na and at −0.3 to −0.4 km for Fe (see Fig. 4a), while the peaks on the layer top sides are respectively at 1.2 to 1.4 km for Na and at 0.6 to 0.8 km for Fe. These results confirm that the observed density scale height (in magnitude) for Fe is generally smaller than for Na.

2.2 Relationship between Na and Fe variations at fixed altitudes

As the first example, Fig. 5 presents the temporal variations of the Na and Fe densities (5-min resolution) at fixed altitudes between 80.84 and 107.72 km (at every twenty altitude bins) on the night of 27–28 July 2004, which is based on the sequences of the Na and Fe density profiles shown by Yi et al. (2007). For the convenience of comparison, the Na and Fe density values at each altitude have been multiplied respectively by given constant factors. Thus the Na and Fe densities plotted in Fig. 5 have the same ceiling (maximum) at each altitude. As seen from Fig. 5, the temporal variations of the Na and Fe densities show an excellent similarity on the bottommost layer underside between 80.84 and 82.76 km, particularly on small time scale. At higher altitudes from 88.52 to 94.28 km, the Na and Fe density variations are quite different. Above the altitude of 96.20 km, the Na and Fe density variations display a weak correlation. In order to detailedly illustrate the similar feature of the Na and Fe variations on the layer underside, we plot in Fig. 6 the temporal variations of the Na and Fe densities on the layer underside at every four altitude bins (0.384 km). As seen in Fig. 6, the Na and Fe time variations for the lowest 2–3 km (∼28 consecutive lidar range bins lowest in altitude) of the layers show an excellent similarity. At higher altitudes, the similarity falls off. The Na and Fe similarity on the layer bottom side can be expressed approximately by

$$n_{\mathrm{Fe}}(z,t) = c(z)\, n_{\mathrm{Na}}(z,t) \qquad z_{\mathrm{b}} < z < z_{\mathrm{s}} \quad , \tag{1}$$

where $n_{\mathrm{Fe}}(z,t)$ and $n_{\mathrm{Na}}(z,t)$ are the Fe and Na densities, $c(z)$ is an only-altitude-dependent quantity, z_{b} is the altitude of the layer lower boundary and z_{s} is the maximum altitude where the density similarity remains. Figure 7 presents the altitude-dependent correlation coefficient between the Na and Fe densities measured during the night of 27–28 July 2004. The correlation calculation proceeded from the bottom up, starting at an altitude where more than 20 data points were available (equivalent to 100 min) in terms of the density criterion

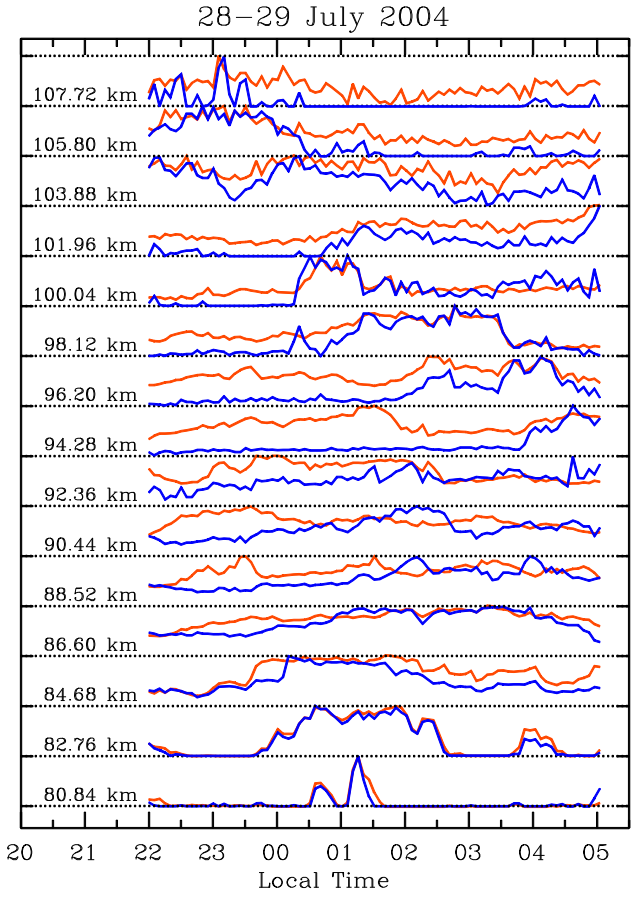

Fig. 5. Time variations of the relative densities for Na (orange line) and Fe (blue line) observed at altitudes between 80.84 and 107.72 km (plotted in every 20 altitude bins) during the night of 28–29 July 2004. Note that the temporal variations of the Na and Fe relative densities show an excellent similarity on the bottommost layer underside between 80.84 and 82.76 km, particularly on small time scale.

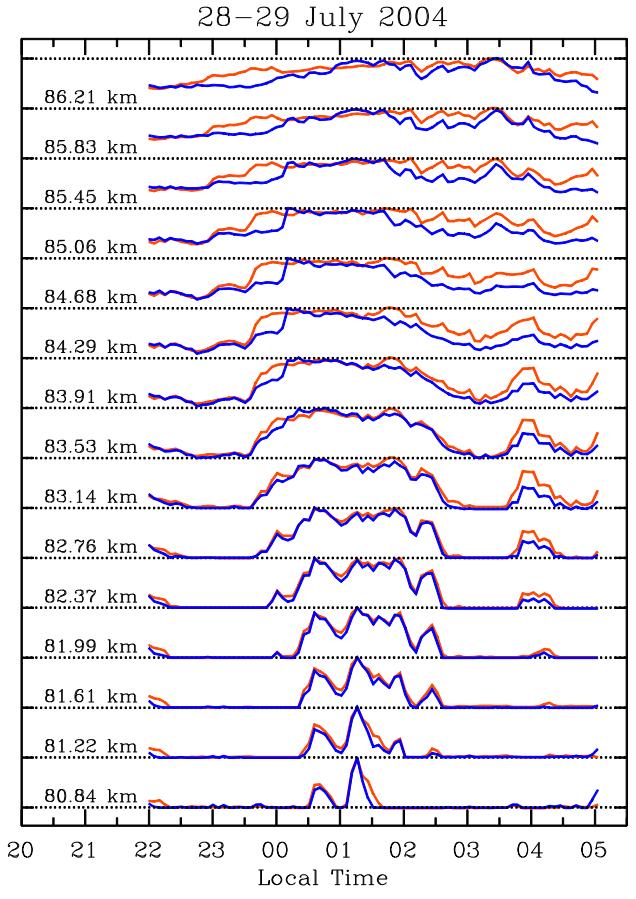

Fig. 6. Time variations of relative densities for Na (orange line) and Fe (blue line) observed at altitudes between 80.84 and 86.21 km (plotted in every 4 altitude bins) during the night of 28–29 July 2004, which display altitude dependence of the Na and Fe time variation relations in detail. Note that the temporal variations of the Na and Fe relative densities show an excellent similarity on the bottommost layer underside, and difference occurs at higher altitudes.

and terminating at an altitude where available data points were less than 20. Since the maximum detection thresholds for all the 5-min Na and Fe density samplings on this night are 13 cm^{-3} and 5 cm^{-3}, respectively, the density criterion is uniformly taken to be 30 cm^{-3} for both Na and Fe. As seen in Fig. 7, the correlation coefficient is larger than 0.9 in the lowest ~3.2 km of the layer with a maximum of 0.99 at 82.3 km. The Na density exhibits a negative correlation with the Fe density in a ~2.8 km altitude range centered near 90 km. The large positive correlation occurs again in a higher altitude range centered around ~97 km. Here we define a similar variation range (SVR) on the layer underside as an altitude range where the correlation coefficient between the Na and Fe densities is greater than or equal to 0.9. As mentioned above, the value of the SVR for this summer night is ~3.2 km.

Figures 8 and 9 give an example from wintertime (on the night of 8–9 December 2004). Like the first example from summertime (Figs. 5 and 6), the Na and Fe densities on the winter night also display an identical temporal variation at altitudes on the bottommost layer underside (Fig. 9). The similarity fades away with increasing altitude. The correlation coefficient between the Na and Fe densities is plotted versus altitude in Fig. 10. Although it displays a complicated wave-like structure in altitude, the essential features still remain unaltered like the first example: the highest positive correlation appears on the bottommost layer underside; a negative correlation occurs in altitude range centered near 90 km; a strong positive correlation arises again in a higher altitude range (~100 km). The SVR for this winter night is ~4.6 km.

In order to ascertain whether nearly the same time variations of the Na and Fe densities on the bottommost layer underside are ubiquitous, we have surveyed all the 47 nights

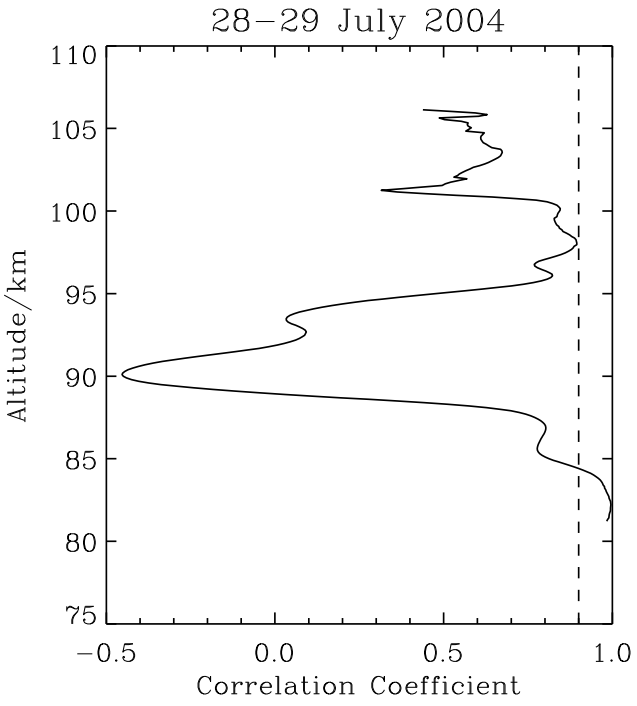

Fig. 7. Correlation coefficient between simultaneously observed Na and Fe densities versus altitude on the night of 28–29 July 2004.

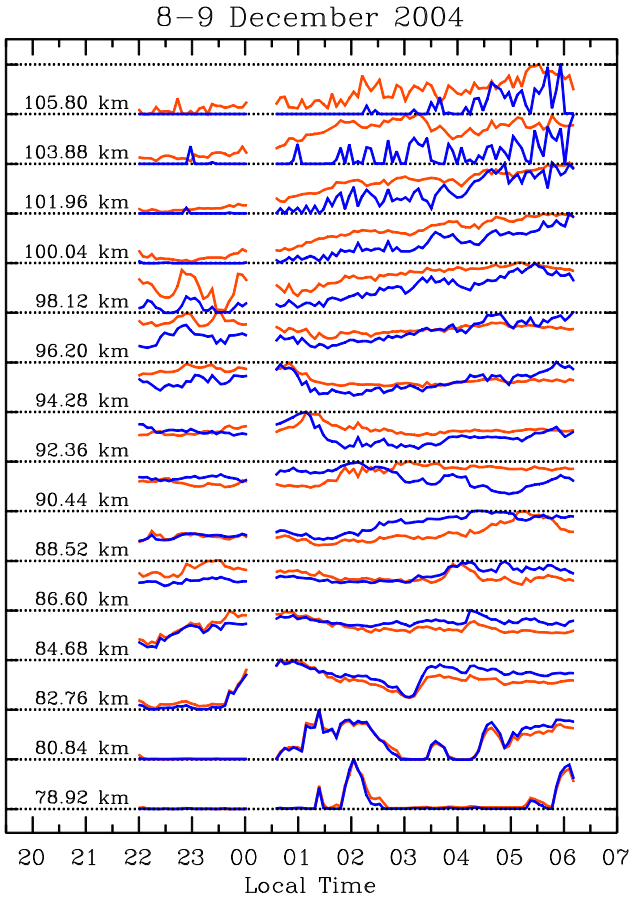

Fig. 8. Time variations of the relative densities for Na (orange line) and Fe (blue line) observed at altitudes between 78.92 and 105.80 km (plotted in every 20 altitude bins) during the night of 8–9 December 2004. Note that the temporal variations of the Na and Fe relative densities show an excellent similarity on the bottommost layer underside between 80.84 and 82.76 km, particularly on small time scale.

of the Na and Fe density data obtained by the simultaneous and common-volume Na and Fe lidar measurements at our site near 30° N. It is found that out of a total of 47 nights, 40 nights (85 %) have correlation coefficients on the bottommost layer underside larger than 0.9. The maximum values of the correlation coefficients on the bottommost layer underside for the remaining 7 nights range from 0.80 to 0.89 with a mean of 0.86. Noting that the nights with the correlation coefficients less than 0.9 generally have the maximum detection thresholds close to 200 cm^{-3}, we believe that the slightly lower correlations for the 7 nights result from lower lidar signal-to-noise ratios. The statistical result confirm that nearly the same time variations of the Na and Fe densities on the bottommost layer underside are a ubiquitous geophysical phenomenon. In terms of our calculation, the SVR for the 40 nights with high correlations on the bottommost layer underside varies from 0.2 to 8.5 km with a mean value of 3.5 km. It is also observed that out of the total 47 nights of the altitude-dependent correlation coefficients, 30 nights (∼63 %) exhibit negative correlations (with the minimum correlation coefficients from −0.30 to −0.91) in an altitude range around 90 km. For the remaining 17 nights, low correlation (with the minimum correlation coefficients from −0.29 to 0.35) is discerned in an altitude range near 90 km. This indicates that the significant distinction between the Na and Fe time variations generally appears in an altitude range near 90 km. In addition, as noticed from all the altitude-dependent correlation coefficients, 40 nights (85 %) out of the total 47 nights display obvious positive correlations in the higher altitude range centered near 100 km with correlation coefficients between 0.60 and 0.98. A weak positive correlation (0.42–0.59) is also discerned from the remaining 7 nights. Hence, a relatively weak positive correlation between the simultaneous Na and Fe data exists in the altitude range near 100 km. The altitude-dependent correlation between Na and Fe densities might be possibly related to the vertical gradients of the mean Na and Fe layers. The positive correlations occur on the low and high layer borders where the Na and Fe gradient values have the same signs, while the negative correlation arises in the altitude region near 90 km where the gradient values for the two species are opposite. Figure 11 gives the altitude profile of the mean correlation coefficient derived from all the 47-night Na and Fe data. It is obtained also by taking the medians of the 47-night correlation coefficients at each altitude bin. As seen in Fig. 11, the

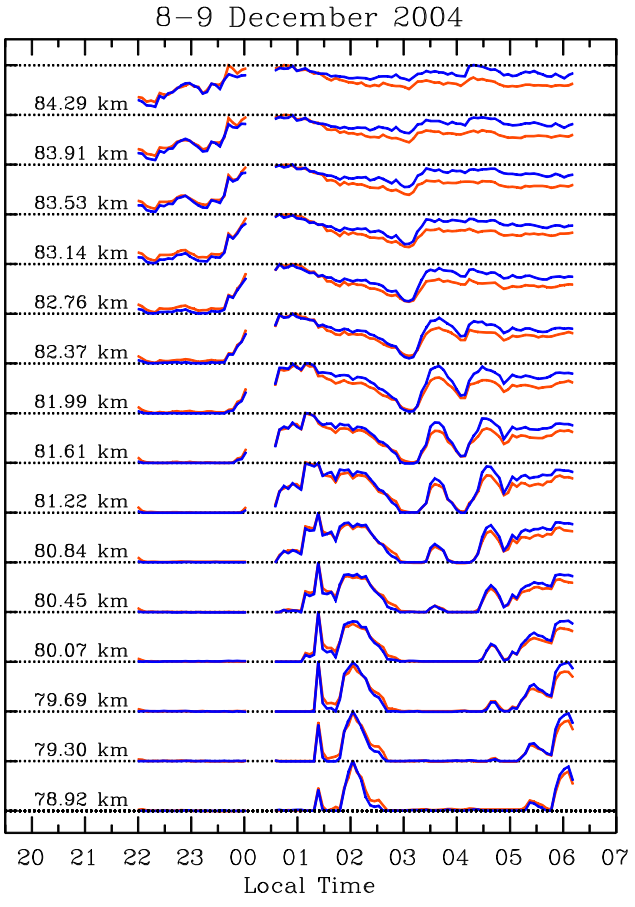

Fig. 9. Time variations of relative densities for Na (orange line) and Fe (blue line) observed at altitudes between 78.92 and 84.29 km (plotted in every 4 altitude bins) during the night of 8–9 December 2004, which display altitude dependence of the Na and Fe time variation relations in detail. Note that the temporal variations of the Na and Fe relative densities show an excellent similarity on the bottommost layer underside, and difference occurs at higher altitudes.

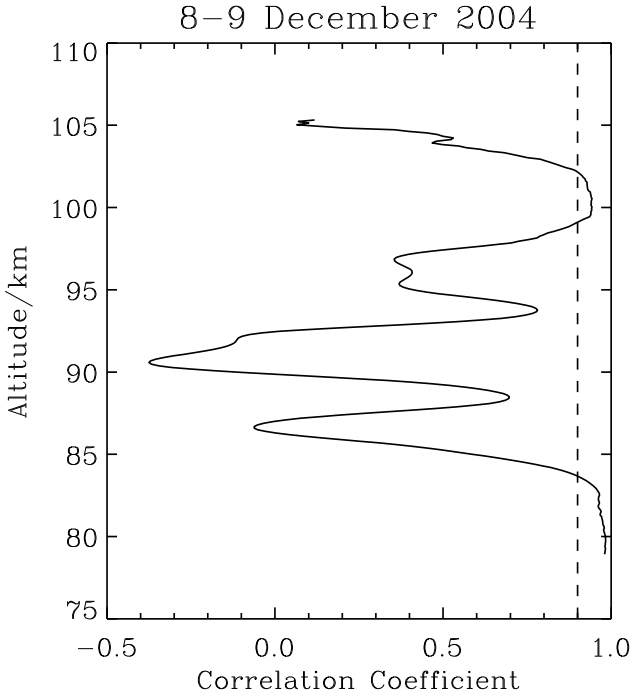

Fig. 10. Correlation coefficient between simultaneously observed Na and Fe densities versus altitude on the night of 8–9 December 2004.

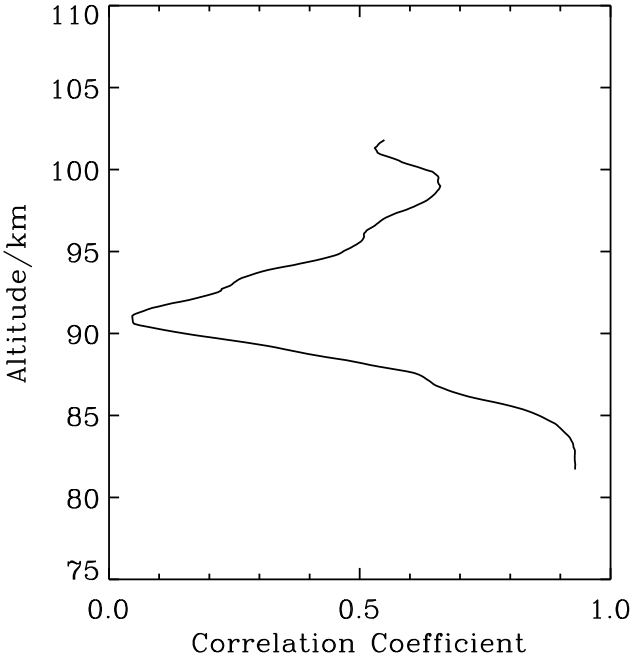

Fig. 11. Mean correlation coefficient between simultaneously-observed Na and Fe densities versus altitude derived from all the 47 nights. The correlation coefficient is smoothed with running mean over 1.4 km.

mean Na-Fe correlation coefficient has a value of ∼0.93 in the lowest several kilometers of the layers, while the corresponding SVR is 2.5 km. The correlation coefficient declines to ∼0.045 at ∼91.0 km. It attains its secondary maximum of 0.66 at ∼98.9 km. As a whole, the altitude dependence of the mean correlation coefficient coincides with that for individual nights, but some features (e.g., larger correlation coefficient values and broader SVR) become slightly weak because of considerable change in the altitude dependence from night to night.

2.3 Density increase and decrease rates for Na and Fe

In order to understand the small-time-scale variations of the Na and Fe layers, here we examine the instantaneous Na and Fe increase and decrease rates at fixed altitudes based on the 5-min Na and Fe density profiles.

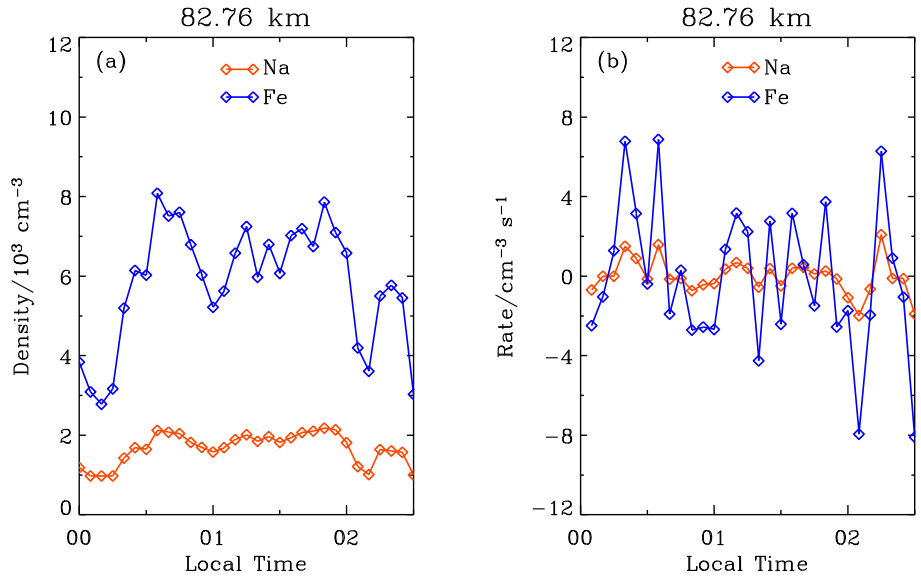

Fig. 12. (a) Time variations of Na and Fe densities and **(b)** Na and Fe variation rates at 82.76 km from 00:00 LT to 02:30 LT on the night of 28–29 July 2004.

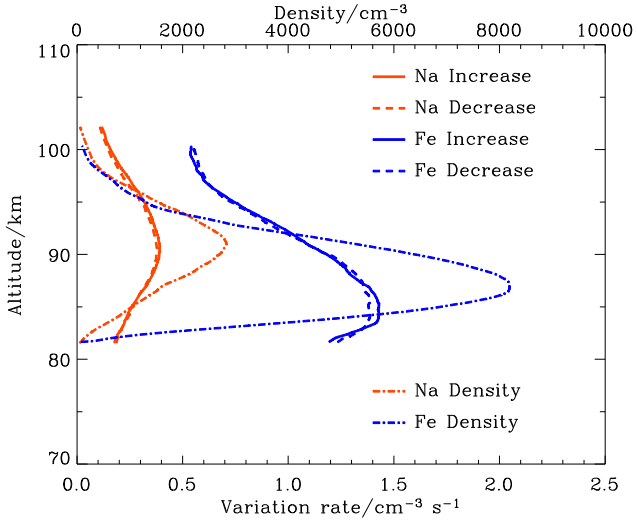

Fig. 13. Profiles of the mean increase and decrease rates for both Na and Fe. The profiles have been smoothed with running mean over 4.8 km in altitude. For comparison, the mean Na and Fe density profiles are presented.

Figure 12 presents an example of the calculated variation rates of the Na and Fe layers together with time variations of their densities at 82.7 km during the night of 28–29 July 2004. Fe has evidently stronger variation rates compared with Na. The Fe increase rate varies from ∼0.3 to ∼6.9 atoms cm^{-3} s^{-1}, while the Fe decrease rate ranges between ∼0.4 and ∼8.1 atoms cm^{-3} s^{-1}. For Na, the increase rate varies from ∼0.1 to ∼2.1 atoms cm^{-3} s^{-1}, while the decrease rate ranges between ∼0.01 and ∼2.0 atoms cm^{-3} s^{-1}.

The magnitude of the variation rates shown in Fig. 12b is a measure of the metal layer variability (regardless of local production/loss or advection effect of already-existing horizontal structure by large-scale wind). In order to further reveal the metal layer variability, we plot in Fig. 13 the profiles of the mean increase and decrease rates for both Na and Fe. The mean variation rate profiles are derived in terms of the following procedure: (1) individual variation rate profiles (Na or Fe) for a given night are obtained via a difference calculation with two adjacent 5-min density profiles. At a given altitude, the positive and negative rate values are respectively gathered together to form increase and decrease rate data subsets. The mean increase and decrease rate values are attained by respectively taking the medians of the two rate subsets. The calculated results at all altitudes on this night are put together to produce the nightly mean profiles of the increase and decrease rates. (2) The annual mean profiles of the increase and decrease rates are acquired by taking the medians of the 47 nightly mean profiles for the increase and decrease rates respectively. Note that a median value is employed instead of an arithmetic mean in all average calculations because it ignores possible extreme rate values. As seen in Fig. 13, the mean increase and decrease rates for both Na and Fe are altitude dependent and have a single-peak structure. The rate magnitudes for both Na and Fe are larger on the layer bottom side than on the layer top side. This coincides with the fact that the observed layer bottoms often show steep gradient and significant vertical displacements (Yi et al., 2008). The mean increase and decrease rates for Na have maxima of 0.39 and 0.37 cm^{-3} s^{-1} at altitudes around 91.2 km, while the corresponding values for Fe are 1.43 and 1.39 cm^{-3} s^{-1} at altitudes near 84.4 km.

Note that the peak altitude of the mean Na increase and decrease rates is 0.4 km lower than that of the mean Na layer, for Fe this altitude is 2.7 km lower than that of the mean Fe layer. The difference between the maximum increase and decrease rates is $+0.02$ for Na and $+0.04\,\mathrm{cm^{-3}\,s^{-1}}$ for Fe. The positive small difference values suggest that each of the Na and Fe densities at such altitudes mostly has a slow net increase during night (because our lidar data were collected only during night). In fact, the difference values between the layer-column-abundance increase and decrease rates (i.e., altitude integration of the change rates shown in Fig. 13) are also positive for both Na and Fe. This is in good agreement with the observed fact that the annual mean Na column abundance show a monotonic increase during night (States and Gardner, 1999). In order to explicitly represent the timescale of the layer variability, we calculate the characteristic time (time constant) in terms of the data plotted on Fig. 13 (which is obtained by the mean density divided by the mean increase/decrease rate). The characteristic time for the Na variability is between $\sim$0.07 and $\sim$2.0 h, while this quantity for Fe ranges from $\sim$0.02 to $\sim$1.7 h. This indicates that the small-scale processes dominate the variability of the Na and Fe layers. The positive small differences between the altitude-integrated increase and decrease rates (derived from Fig. 13) yield quite large characteristic time values for both Na and Fe. They reflect a slow net increase in each of the annual mean Na or Fe column abundances during night.

3 Conclusion and discussion

The average properties and small-scale variation features of the mesospheric Na and Fe layers at 30° N have been revealed based on the extensive simultaneous and common-volume Na and Fe lidar measurements at Wuhan, China. In terms of the averaging approach of Tilgner and von Zahn (1988), the annual mean Na and Fe density profiles are derived from a total of $\sim$268 h simultaneous Na and Fe density data on 47 different nights. It is shown that the mean Na and Fe layers have much steeper density gradients on the bottom side than on the top side, and the borders of the Fe layer are obviously steeper than those of the Na layer. Near the bottommost of the annual mean layers the Na and Fe scale heights are respectively -0.42 and -0.30 km, while at the topside of the mean layers (at 103 km for Na and 101 km for Fe) the corresponding values are 1.06 and 0.82 km. Both the Na and Fe scale heights on the layer bottom sides are obviously smaller in magnitude than those derived from the conventional arithmetic average ($<$2 km for Na and $<$1 km for Fe) (Plane, 2003).

The Na and Fe densities in the lowest several kilometers of the layers consistently exhibit nearly the same time variations. According to our statistics, on 40 nights (85 %) out of a total of 47 nights, the correlation coefficients between the Na and Fe densities are larger than 0.9 on the layer undersides. The remaining 7 nights have the maximum correlation coefficients ranging from 0.80 to 0.89 on the layer undersides. The slightly lower correlations for the 7 nights result from lower lidar signal-to-noise ratios. At higher altitudes, the similarity falls off. A clear-cut distinction between the Na and Fe time variations usually appears in an altitude range near 90 km. There is a relatively weak positive correlation between the simultaneous Na and Fe data in an altitude range near 100 km.

For each metal atom species (Na or Fe), the mean increase and decrease rates are altitude dependent and have a single-peak structure. In addition, the rate magnitudes for both Na and Fe are larger on the layer bottom side than on the layer top side. This coincides with the fact that the observed layer bottoms often show steep gradient and significant vertical displacements. For each metal species (Na or Fe), the difference between the increase and decrease rates of the layer column abundance is a small positive value. This indicates that each of the Na and Fe column abundances mostly has a slow net increase during night. The peak altitude of the mean Na increase/decrease rates is 0.4 km lower than that of the mean Na layer, for Fe this altitude is 2.7 km lower than that of the mean Fe layer. The characteristic time for the Na variability ranges from $\sim$0.07 and $\sim$2.0 h, while this quantity for Fe varies from $\sim$0.02 and $\sim$1.7 h. Obviously the small-scale processes dominate the variability of the Na and Fe layers. However, there exists also a slow net increase in each of the annual mean Na and Fe column abundances during night.

Introducing the gravity wave perturbation (a monochromatic wave) in the Na and Fe models (via temperature and minor species concentrations), Plane et al. (1999a) simulated the kinetic response of the Na and Fe atoms for two wave periods. Their calculations showed that, below 84 km the Fe/Na ratio at given altitude varies by a factor of 5, whereas between 87 and 100 km the ratio varies by no more than a factor of 2, as the wave propagates. In terms of model analysis, on the layer underside, Fe undergoes significant chemical amplification, but Na does not because the different chemical reactions control their undersides (Plane et al., 1999a). Obviously the modeled results are different with the observed ubiquitous relationship between Na and Fe variations at fixed altitudes, particularly the fact that on the layer underside the Na and Fe densities vary with a nearly constant Fe/Na ratio at given altitude.

As mentioned above, the observed Na and Fe lower boundaries always follow nearly the same movements and show consistently a delicate stratification with the Fe lower boundary being in general slightly higher than or coincident with that of the Na layer (Yi et al., 2007, 2008). Atmospheric gravity waves so far are generally believed to induce the vertical movements. But, at the lower boundaries near 80 km altitude the vertical mixing of constituents by turbulence generated (or brought) by gravity waves tends to spoil the stratification. It appears that gravity waves alone cannot explain the always-existing delicate stratification under the modulation

of the vertical movements. Obviously, ascertaining the complicated physics behind the simultaneously-observed Na and Fe characteristics needs further observational and modeling efforts.

In terms of the airglow observations, the peak altitudes of the perturbations in the OH and O_2 volume emission rates are respectively a few kilometers lower than that of the corresponding unperturbed emissions (Swenson and Gardner, 1998; Liu and Swenson, 2003). Considering that the variation (increase/decrease) rate magnitude is equivalent to the perturbation intensity, this feature appears to be similar to our current lidar observations that the peak altitude of the mean variation rate is lower than that of the mean layer for both Na and Fe. However, the metal atoms (Na and Fe) apparently differ in chemistry from hydroxyl and molecular oxygen. Thus, further work in both observation and modeling is required to clarify this nearly universal feature for the layered phenomena in the mesosphere.

Acknowledgements. The research is supported jointly by the National Natural Science Foundation of China through grants 40874081 and 40731055 and Ocean Public Welfare Scientific Research Project from State Oceanic Administration, People's Republic of China (No. 201005017). The authors appreciate Yunpeng Zhang and Changming Yu for their technical assistance and support in collecting lidar data.

Topical Editor C. Jacobi thanks two anonymous referees for their help in evaluating this paper.

References

Alpers, M., Höffner, J., and von Zahn, U.: Iron atom densities in the polar mesosphere from lidar observations, Geophys. Res. Lett., 17, 2345–2348, 1990.

Bills, R. E. and Gardner, C. S.: Lidar observations of mesospheric Fe and sporadic Fe layers at Urbana, Illinois, Geophys. Res. Lett., 17, 143–146, 1990.

Bowman, M. R., Gibson, A. J., and Sandford, M. C. W.: Atmospheric sodium measured by a tuned laser radar, Nature, 221, 456–457, 1969.

Clemesha, B. R., Kirchhoff, V. W. J. H., and Simonich, D. M.: Concerning the seasonal-variation of the mesospheric sodium layer at low-latitudes, Planet. Space Sci., 27, 909–910, 1979.

Eska, V., von Zahn, U., and Plane, J. M. C.: The terrestrial potassium layer (75–110 km) between 71° S and 54° N: Observations and modeling, J. Geophys. Res., 104, 17173–17186, 1999.

Gardner, C. S.: Sodium resonance fluorescence lidar applications in atmospheric science and astronomy, Proc. IEEE, 77(3), 408–418, 1989.

Gardner, C. S., Plane, J. M. C., Pan, W., Vondra, T., Murray, B. J., and Chu, X.: Seasonal variations of the Na and Fe layers at the South Pole and their implications for the chemistry and general circulation of the polar mesosphere, J. Geophys. Res., 110, D10302, doi:10.1029/2004JD005670, 2005.

Gardner, C. S., Chu, X., Espy, P. J., Plane, J. M. C., Marsh, D. R., and Janches, D.: Seasonal variations of the mesospheric Fe layer at Rothera, Antarctica (67.5° S, 68.0° W), J. Geophys. Res., 116, D02304, doi:10.1029/2010JD014655, 2011.

Gerding, M., Alpers, M., von Zahn, U., Rollason, R. J., and Plane, J. M. C.: Atmospheric Ca and Ca^+ layers: Midlatitude observations and modeling, J. Geophys. Res., 105, 27131–27146, 2000.

Heide, F. and Wlotzka, F.: Meteorites: Messengers from space, Springer-Verlag, Berlin, Heidelberg, 1995.

Heinselman, C. J.: Auroral effects on meteoric metals in the upper atmosphere, PhD dissertation, Stanford Univ., Stanford, Calif, 1999.

Helmer, M., Plane, J. M. C., Qian, J., and Gardner, C. S.: A model of meteoric iron in the upper atmosphere, J. Geophys. Res., 103, 10913–10925, 1998.

Kane, T. J. and Gardner, C. S.: Structure and seasonal variability of the nighttime mesospheric Fe layer at midlatitudes, J. Geophys. Res., 98, 16875–16886, 1993.

Liu, A. Z. and Swenson, G. R.: A modeling study of O_2 and OH airglow perturbations induced by atmospheric gravity waves, J. Geophys. Res., 108, D4, doi:10.1029/2002JD002474, 2003.

Liu, Y. and Yi, F.: Behavior of sporadic Na layers on small time scale, J. Atmos. Sol. Terr. Phys., 71, 1374–1382, doi:10.1016/j.jastp.2009.06.013, 2009.

Lynch, K. A., Gelinas, L. J., Kelley, M. C., Collions, R. L., Widholm, M., Rau, D., MacDonald, E., Liu, Y., Ulwick, J., and Mace, P.: Multiple sounding rocket observations of charged dust in the polar winter mesosphere, J. Geophys. Res., 110, A03302, doi:10.1029/2004JA010502, 2005.

Ma, Z. and Yi, F.: High-altitude sporadic metal atom layers observed with Na and Fe lidars at 30° N, J. Atmos. Sol. Terr. Phys., 72, 482–491, doi:10.1016/j.jastp.2010.01.005, 2010.

Megie, G. and Blamont, J. E.: Laser sounding of atmospheric sodium: Interpretation in terms of global atmospheric parameters, Planet. Space Sci., 25, 1093–1109, 1977.

Plane, J. M. C.: Atmospheric Chemistry of meteoric metals, Chem. Rev., 103, 4963–4984, 2003.

Plane, J. M. C.: A time-resolved model of the mesospheric Na layer: constraints on the meteor input function, Atmos. Chem. Phys., 4, 627–638, doi:10.5194/acp-4-627-2004, 2004.

Plane, J. M. C., Cox, R. M., and Rollason, R. J.: Metallic layers in the mesopause and lower thermosphere region, Adv. Space Res., 24(11), 1559–1570, 1999a.

Plane, J. M. C., Gardner, C. S., Yu, J., She, C. Y., Garcia, R. R., and Pumphrey, H. C.: Mesospheric Na layer at 40° N: Modeling and observations, J. Geophys. Res., 104, 3773–3788, 1999b.

She, C. Y., Chen, S. S., Hu, Z. L., Sherman, J., Vance, J. D., Vasoli, V. M., White, A., Yu, J. R., and Krueger, D. A.: Eight-year climatology of nocturnal temperature and sodium density in the mesopause region (80 to 105 km) over Fort Collins, CO (41° N, 105° W), Geophys. Res. Lett., 27, 3289–3292, doi:10.1029/2000GL003825, 2000.

Shibata, Y., Nagasawa, C., Abo, M., Maruyama, T., Saito, S., and Nakamura, T.: Lidar observations of sporadic Fe and Na layers in the mesopause region over Equator, J. Meteorol. Soc. of Japan, 84A, 317–325, 2006.

Simonich, D. M., Clemesha, B. R., and Kirchhoff, V. W. J. H.: The mesospheric sodium layer at 23° S: Nocturnal and seasonal variations, J. Geophys. Res., 84, 1543–1550, 1979.

States, R. J. and Gardner, C. S.: Structure of the mesospheric Na layer at 40° N latitude: Seasonal and diurnal variations, J. Geophys. Res., 104, 11783–11798, 1999.

Swenson, G. R. and Gardner, C. S.: Analytical models for the re-

sponses of the mesospheric OH* and Na layers to atmospheric gravity waves, J. Geophys. Res., 103, 6271–6294, 1998.

Tilgner, C. and von Zahn, U.: Average properties of the sodium density distribution as observed at 69° N latitude in winter, J. Geophys. Res., 93, 8439–8454, 1988.

Yi, F., Zhang, S. D., Zeng, H. J., He, Y. J., Yue, X. C., Liu, J. B., Lv, H. F., and Xiong, D. H.: Lidar observations of sporadic Na layers over Wuhan (30.5° N, 114.4° E), Geophys. Res. Lett., 29(9), 1345, doi:10.1029/2001GL014353, 2002.

Yi, F., Zhang, S., Yu, C., He, Y., Yue, X., Huang, C., and Zhou, J.: Simultaneous observations of sporadic Na and Fe Layers by two closely colocated resonance fluorescence lidars at Wuhan (30.5° N, 114.4° E), China, J. Geophys. Res., 112, D04303, doi:10.1029/2006JD007413, 2007.

Yi, F., Zhang, S., Yue, X., He, Y., Yu, C., Huang, C., and Li, W.: Some ubiquitous features of the mesospheric Na and Fe layer borders from simultaneous and common-volume Na and Fe lidar observations, J. Geophys. Res., 113, A04S91, doi:10.1029/2007JA012632, 2008.

Yi, F., Yu, C., Zhang, S., Yue, X., He, Y., Huang, C., Zhang, Y., and Huang, K.: Seasonal variations of the nocturnal mesospheric Na and Fe layers at 30° N, J. Geophys. Res., 114, D01301, doi:10.1029/2008JD010344, 2009.